https://doi.org/10.20965/jrm.2024.p0483

Paper:

An Admittance Controller with a Jerk Limiter for Position-Controlled Robots

Ryusei Mae and Ryo Kikuuwe

Machinery Dynamics Laboratory, Hiroshima University
1-4-1 Kagamiyama, Higashi-hiroshima, Hiroshima 739-8527, Japan
E-mail: mae@mdl.hiroshima-u.ac.jp
[Received July 3, 2023; accepted January 31, 2024]

This paper proposes an admittance control scheme for robots equipped with joint-level position controllers involving deadtime. Its main feature is an elaborate discrete-time jerk limiter, which limits the third derivative of the position command sent to the controller. The jerk limiter is designed to suppress undesirable oscillation especially when the robot is in contact with a stiff environment. The controller is designed as a differential inclusion involving normal cones in the continuous-time domain, and its discrete-time algorithm is derived by the implicit Euler discretization. The presented controller was validated with experiments using a collaborative robot UR3e of Universal Robots, which has a deadtime of 6 ms in the velocity-command mode.

Keywords: admittance control, jerk limiter, vibration suppression, normal cone, differential inclusion

1. Introduction

Robots subject to physical contact with external environments need appropriate controllers to regulate the contact forces. Most industrial robots are controlled by proprietary, dedicated position controllers that force the robots to track position commands from upper-level controllers. To enable such a robot to respond to external forces, an additional controller is needed to modify the position commands according to the contact forces.

Admittance control is a control scheme that is suited for position-controlled robot manipulators. It is often referred to as position-based impedance control, and it can be implemented as an outer feedback loop attached to a position-controlled system. In an admittance controller, a virtual object having desired inertia, viscosity, and stiffness is considered, and its motion is simulated according to the external force obtained from a force sensor or some estimation methods. The robot is then position-controlled to track the motion of the virtual object.

One problem of admittance control is instability. The robot may become unstable, especially when it is in contact with a stiff environment and when the time delay in the controller is large [1]. It is known that admittance control can be stabilized by setting high values to the viscosity and inertia of the virtual object [1], but it would deteriorate the responsiveness against the external forces. Some strategies have been proposed to adaptively vary the viscosity and inertia parameters of admittance control [2–11]. The trade-off between stability and responsiveness, however, is still inevitable in these methods. Current velocity feedback [12], which injects additional damping into the system, has been shown to be effective in enhancing the stability, but it would also deteriorate the responsiveness.

It has been known [13–15] that the feedforward of the target acceleration in the position controller enhances the stability. However, it is not applicable to most commercially-available manipulators because they usually do not provide access to the internal algorithms of their position controllers. Some researchers [16–18] employed fractional-order dynamics for admittance controller. It has been reported [16] that it contributes to better stability in comparison to the integer-order counterparts. Its efficacy, however, is still theoretically unclear and its physical interpretation is complicated, possibly leading to difficulties in parameter tuning.

There have also been approaches to reduce the risk of instability and vibration by limiting the actuator torque [14] and the commanded acceleration [13–15]. They are also strongly coupled with the internal position controllers and are not very straightforward to use with commercial position-controlled robots, of which the internal controller structures are not disclosed. An approach to alter the commanded acceleration to enhance the stability has been studied [19], but it is also coupled with the internal position controller and its effectiveness in the presence of the time delay is unclear. Imposing limits to the commanded velocity and acceleration has also been studied in [20], but it is primarily intended for enhancing safety, not for the stability.

This paper proposes an admittance control scheme with a jerk limiter for position-controlled robots. The novelty of the proposed admittance controller is that it has a jerk limiter, which limits the third derivative of the position command sent to the robot. The jerk limiter is shown to be effective in suppressing the vibration that happens when the robot is in contact with a stiff environment. It has a structure that adjusts the jerk limit according to the velocity and the acceleration in order not to sacrifice the

responsiveness to external forces. The vibration caused by the instability is suppressed by limiting the first, second, and third derivatives of the position command. One of its practical benefits is that it suppresses the vibrations even if the virtual viscosity and virtual inertia are set low. Another advantage is that it is applicable without the knowledge of the structure of the internal position controller of the robot. The effectiveness of the proposed method is verified by some experiments using a collaborative robot UR3e.

The remainder of this paper is organized as follows. Section 2 provides some mathematical preliminaries. Section 3 details the proposed admittance controller. Section 4 presents the experimental results obtained by implementing the proposed controller on a UR3e robot. Section 5 concludes this paper.

2. Mathematical Preliminaries

Let a, b, and x be real numbers and $a \leq b$. This paper uses the following functions:

$$\mathrm{proj}_{[a,b]}(x) \triangleq \begin{cases} b, & \text{if } b < x; \\ x, & \text{if } a \leq x \leq b; \\ a, & \text{if } x < a, \end{cases} \quad \ldots\ldots (1)$$

$$\mathrm{dzn}_{[a,b]}(x) \triangleq x - \mathrm{proj}_{[a,b]}(x), \quad \ldots\ldots (2)$$

$$\mathcal{N}_{[a,b]}(x) \triangleq \begin{cases} (-\infty, 0], & \text{if } x = a; \\ 0, & \text{if } a < x < b; \\ [0, \infty), & \text{if } x = b; \\ \emptyset, & \text{if } x > b \vee x < a. \end{cases} \quad \ldots (3)$$

The functions proj and dzn can be referred to as the projection and deadzone functions, respectively. The function $\mathcal{N}$ is called the normal cone [21]. The following relation exists between the projection function and the normal cone:

$$y \in x - \mathcal{N}_{[a,b]}(y) \iff y = \mathrm{proj}_{[a,b]}(x), \quad \ldots (4)$$

which has been shown in previous publications (e.g., ([22], Proposition 2), ([23], Section A.3), and ([24], Proposition 6.47)).

3. Proposed Method

3.1. Conventional Admittance Controller

Figure 1(a) is an example of the structure of an admittance controller. The controller comprises a virtual object, often referred to as a *proxy*, and the robot is position- or velocity-controlled to track the proxy position. The proxy moves according to a predetermined equation of motion, a typical example of which can be described as follows:

$$M(\ddot{q} - \ddot{p}_d) + B(\dot{q} - \dot{p}_d) + K(q - p_d) = f + f_d, \quad (5)$$

where q is the proxy position and f is the force acting on the robot, which is obtained from a force sensor or other means. The quantities p_d and f_d are the desired position and the desired force, respectively, given as inputs to the controller, and M, B, and K are positive constants representing the inertia, viscosity, and stiffness, respectively. As long as the position controller is accurate enough, the robot's response to the external force f is close to the proxy dynamics described by Eq. (5).

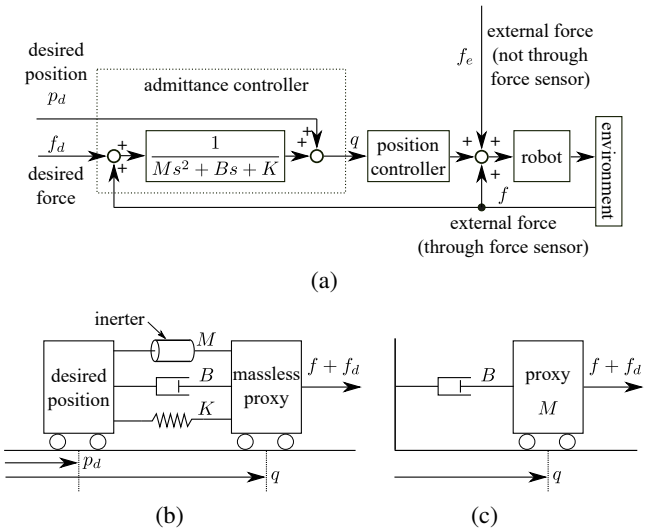

Fig. 1. System controlled with admittance controller. (a) Typical admittance controller. (b) A physical interpretation of the proxy dynamics (Eq. (5)). (c) A physical interpretation of the proxy dynamics (Eq. (5)) with $K = 0$ and $\dot{p}_d \equiv 0$.

One interpretation of the proxy dynamics (Eq. (5)) can be illustrated in **Fig. 1(b)**. Here, the proxy can be considered as a massless object and is connected to the desired position p_d through a parallel spring-damper-inerter element.[1] The forces f and f_d act on the proxy. The proxy dynamics of this form can be used, for example, when the robot should track the desired position p_d with a certain level of compliance against the external force f, by deviating from the desired position p_d. In such an application, the desired force f_d should usually be set to be constantly zero, and the parameters should also be set to satisfy $B^2 > 4KM$ to prevent overshoots.

One variation of the controller can be obtained by setting $K = 0$ and $\dot{p}_d \equiv 0$ with the proxy dynamics (Eq. (5)). In such a case, the proxy dynamics reduces to the one illustrated in **Fig. 1(c)**, in which the proxy is a point mass combined with a damper subject to the forces f and f_d. Such a controller can be used, for example, when the robot should yield to the external force, such as the one applied by a human user in the case of direct teaching, or when the robot should apply the force f_d to an external object in the case of grinding or assembly tasks.

It is well known that admittance-controlled systems are prone to instability, especially when the robot is in contact with an external object. As has been discussed in previous work (e.g., [14, 15]), the cause of the instability is the phase lag or the deadtime in the closed loop.

1. This paper uses the term inerter to mean an element that produces the force proportional to the relative acceleration between its two ends.

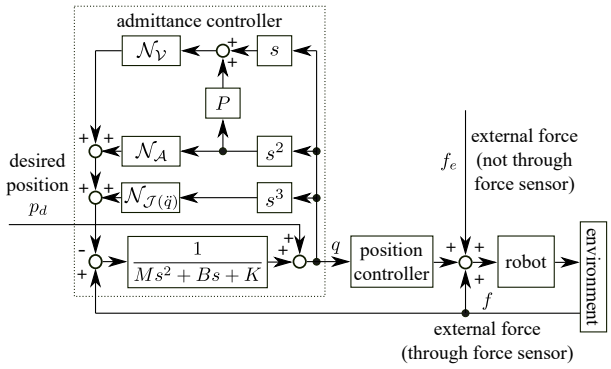

Fig. 2. System controlled with proposed admittance controller.

One approach to compensate for the phase lag is to use phase-leading and acceleration feedforward techniques in the position controller [15]. The effect of instability can be attenuated by imposing limits on the actuator torque [14]. These approaches need to alter the structure of the position controllers and thus are not applicable to commercial robot manipulators equipped with proprietary position controllers. Moreover, it is questionable whether these methods are applicable to deadtime of more than a few milliseconds, which can exist in commercial position controllers.

3.2. Proposed Admittance Controller

As an extension of the typical admittance controller (Eq. (5)), this paper proposes an admittance controller that can be written as follows:

$$M(\ddot{q}-\ddot{p}_d)+B(\dot{q}-\dot{p}_d)+K(q-p_d) \in f-\mathcal{N}_\mathcal{V}(\dot{q}+P\ddot{q})-\mathcal{N}_\mathcal{A}(\ddot{q})-\mathcal{N}_{\mathcal{J}(\ddot{q})}(\dddot{q}), \quad . \quad (6)$$

where

$$\mathcal{V} \triangleq [-V, V], \quad . \quad (7a)$$

$$\mathcal{A} \triangleq [-A, A], \quad . \quad (7b)$$

$$\mathcal{J}(\ddot{q}) \triangleq \left[\mathrm{proj}_{[-J,-J_y]}\left(-J_s-H\ddot{q}\right), \mathrm{proj}_{[J_y,J]}\left(J_s-H\ddot{q}\right)\right]. \quad . \quad (7c)$$

Here, P, V, A, J, J_s, H, and J_y are positive constants. The proposed controller (6) can be represented by the block diagram in **Fig. 2**.

Mathematical representations like Eq. (6), including "$\in$" instead of "=," are referred to as differential inclusions. The behavior of the differential inclusion (6) can be understood by **Fig. 3**, which shows the three-dimensional space of the vector $[\dot{q}, \ddot{q}, \dddot{q}]^\mathrm{T}$ and the three-dimensional region defined by the following condition:

$$\dot{q}+P\ddot{q}\in\mathcal{V},\ \ddot{q}\in\mathcal{A},\ \dddot{q}\in\mathcal{J}(\ddot{q}). \quad . \quad (8)$$

As long as $[\dot{q}, \ddot{q}, \dddot{q}]^\mathrm{T}$ is in the interior of the region, the last three terms on the right-hand side of Eq. (6) reduce to zero, and Eq. (6) acts as the following ordinary differential equation:

$$M\left(\ddot{q}-\ddot{p}_d\right)+B\left(\dot{q}-\dot{p}_d\right)+K\left(q-p_d\right)=f. \quad . \quad (9)$$

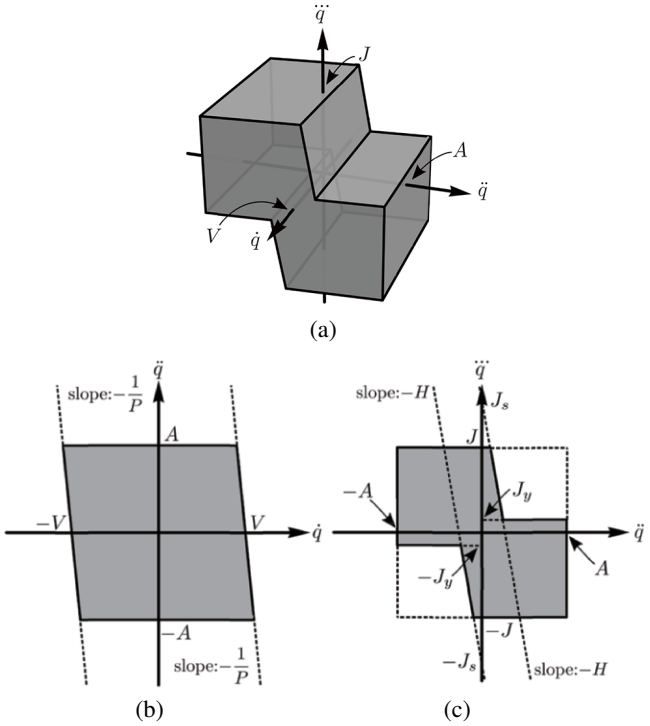

Fig. 3. Illustration of the three-dimensional region within which $[\dot{q}, \ddot{q}, \dddot{q}]^\mathrm{T}$ satisfies the constraint (8). (a) Three-dimensional plot of the region. (b) The cross-section of the region at $\dddot{q} = 0$. (c) The cross-section of the region at $\ddot{q} = 0$.

In other words, if $\{\dot{q}, \ddot{q}, \dddot{q}\}$ determined by Eq. (9) is in the interior of the region, Eq. (6) is equivalent to Eq. (9), which is a spring-damper-inerter system illustrated in **Fig. 1(b)**. On the other hand, if $\{\dot{q}, \ddot{q}, \dddot{q}\}$ determined by Eq. (9) is outside the region (8), $\{\dot{q}, \ddot{q}, \dddot{q}\}$ is chosen as a point on the boundary of the region so that Eq. (6) is satisfied. One would wonder about the existence and the uniqueness of such a solution, but as will be detailed in Section 3.3, the implicit Euler discretization of Eq. (6) always has a unique solution if P and H are chosen appropriately.

The second term on the right-hand side of Eq. (6) is for limiting the velocity, and it is mainly for safety reasons. The term $+P\ddot{q}$ is for realizing the exponential convergence to the velocity limits $\pm V$. As pointed out in [20], a simple velocity limiter without such a term as $+P\dddot{p}$ would cause an abrupt change in the acceleration at the time of reaching the velocity limit, which would not be favorable.

The third and fourth terms on the right-hand side of Eq. (6) aim to reduce the amplitude of the robot's vibration by limiting the commanded jerk $\dddot{q}$. This is motivated by an initial idea that imposing limiters to the commanded acceleration $\ddot{q}$ or the commanded jerk $\dddot{q}$ could be effective in limiting the amplitude of the vibration induced by the instability. Of course, limiters would not eliminate the instability or the vibration in principle as long as deadtime or phase lag exists in the controlled system. Instead, our idea is to reduce the amplitude of the vibration to a practically acceptable level by an appropriate adjustment of the limiters. From preliminary experiments, we found that the

commanded acceleration $\ddot{q}$ was somewhat effective in suppressing the vibration, but it resulted in poor responsiveness of the robot to the external force. In contrast, limiting both the commanded jerk $\dddot{q}$ and the commanded acceleration $\ddot{q}$ was rather effective in realizing both smaller vibration and better responsiveness.

Our observation showed that the vibration could not be sufficiently suppressed only by adjusting the upper bounds A and J, which are for the commanded acceleration and the commanded jerk, respectively. Specifically, when J/A is large, high-frequency oscillations could not be eliminated, but when J/A is small, low-frequency and high-amplitude oscillations took place. The design of the acceleration-dependent jerk limits illustrated in **Fig. 3** is motivated by this observation. The basic idea is that, when the acceleration is high, the jerk limit should be lowered to suppress the high-frequency vibration, but when the acceleration is low, higher jerk values should be allowed to prevent low-frequency, high-amplitude oscillation.

As illustrated in **Fig. 3**, the parameters J_s, J, and J_y should be chosen as $J_y < J < J_s$. The values of A, J, J_s, J_y, and H need to be chosen considering the trade-off between the vibration suppression and the responsiveness to external forces. Specifically, higher A, J, J_y, and J_s, and a smaller H result in higher responsiveness and larger vibration. In particular, the choice of A and J is important because it determines how quickly the robot can start moving from a resting state and how quickly the robot can stop from a moving state when an external force is applied. Once A and J are chosen to maintain the responsiveness, J_y, J_s, and H should be chosen so that the first and third quadrants of the rectangle in **Fig. 3(c)** are significantly notched to suppress the high-frequency vibration. While definitive guidelines for tuning other parameter values are currently unavailable, one can experimentally adjust them through trial and error.

3.3. Discrete-Time Representation

Because the differential inclusion (6) involves the set-valuedness, its implementation to discrete-time controllers is not straightforward. One needs to derive a controller algorithm to obtain the jerk satisfying Eq. (6) at every timestep. We employ the implicit Euler discretization of Eq. (6) to derive a discrete-time controller in a similar manner to those in [13–15], which also used differential inclusions and the implicit Euler discretization in control applications.

The discrete-time representations of Eqs. (6) and (7) are now derived. Let T be the timestep size and k be the integer representing the discrete-time index. Discretizing Eqs. (6) and (7) using the implicit Euler discretization, we obtain the following:

$$M\left(a_k - a_{d,k}\right) + B\left(v_k - v_{d,k}\right) + K\left(q_k - p_{d,k}\right) \in f_k - \mathcal{N}_{\mathcal{V}}\left(v_k + Pa_k\right) - \mathcal{N}_{\mathcal{A}}\left(a_k\right) - \mathcal{N}_{\mathcal{J}(a_k)}\left(j_k\right), \quad (10)$$

where

$$v_k \triangleq \frac{q_k - q_{k-1}}{T}, \quad (11)$$

$$v_{d,k} \triangleq \frac{p_{d,k} - p_{d,k-1}}{T}, \quad (12)$$

$$a_k \triangleq \frac{q_k - 2q_{k-1} + q_{k-2}}{T^2}, \quad (13)$$

$$a_{d,k} \triangleq \frac{p_{d,k} - 2p_{d,k-1} + p_{d,k-2}}{T^2}, \quad (14)$$

$$j_k \triangleq \frac{q_k - 3q_{k-1} + 3q_{k-2} - q_{k-3}}{T^3}. \quad (15)$$

Then, rearranging Eq. (10) so that the commanded jerk j_k appears alone on the left-hand side, we obtain the following:

$$j_k \in j_k^* - \mathcal{N}_{\mathcal{V}}\left(v_k + Pa_k\right) - \mathcal{N}_{\mathcal{A}}\left(a_k\right) - \mathcal{N}_{\mathcal{J}(a_k)}\left(j_k\right), \quad (16)$$

where

$$q_k^* \triangleq p_{d,k} + \frac{(2M + BT)\left(q_{k-1} - p_{d,k-1}\right)}{M + BT + KT^2} - \frac{M\left(q_{k-2} - p_{d,k-2}\right) - T^2 f_k}{M + BT + KT^2}, \quad (17)$$

$$j_k^* \triangleq \frac{q_k^* - 3q_{k-1} + 3q_{k-2} - q_{k-3}}{T^3}. \quad (18)$$

Through the derivation detailed in Appendix A, Eq. (16) can be written as follows:

$$j_k \in j_k^* - \mathcal{N}_{\mathcal{L}_k}\left(j_k\right), \quad (19)$$

where

$$\bar{V}_{b,k} \triangleq \frac{-V - v_{k-1} - (T + P)a_{k-1}}{T^2 + PT}, \quad (20)$$

$$\bar{V}_{t,k} \triangleq \frac{V - v_{k-1} - (T + P)a_{k-1}}{T^2 + PT}, \quad (21)$$

$$\bar{A}_{b,k} \triangleq \frac{-A - a_{k-1}}{T}, \quad (22)$$

$$\bar{A}_{t,k} \triangleq \frac{A - a_{k-1}}{T}, \quad (23)$$

$$\bar{J}_{b,k} \triangleq \mathrm{proj}_{[-J,-J_y]}\left(\frac{-Ha_{k-1} - J_s}{1 + HT}\right), \quad (24)$$

$$\bar{J}_{t,k} \triangleq \mathrm{proj}_{[J_y,J]}\left(\frac{-Ha_{k-1} + J_s}{1 + HT}\right), \quad (25)$$

$$\mathcal{L}_k \triangleq \left[\max\left(\bar{V}_{b,k}, \bar{A}_{b,k}, \bar{J}_{b,k}\right), \min\left(\bar{V}_{t,k}, \bar{A}_{t,k}, \bar{J}_{t,k}\right)\right]. \quad (26)$$

By using the relation (4), Eq. (19) can be written as follow:

$$j_k = \mathrm{proj}_{\mathcal{L}_k}\left(j_k^*\right). \quad (27)$$

This means that Eq. (19), involving the set-valuedness, is equivalently rewritten as Eq. (27), which does not involve set-valuedness. In conclusion, the algorithm of the proposed controllers (6) and (7) can be written as follows:

$$q_k^* := p_{d,k} + \frac{(2M+BT)\left(q_{k-1}-p_{d,k-1}\right)}{M+BT+KT^2}, \\ -\frac{M\left(q_{k-2}-p_{d,k-2}\right)-T^2 f_k}{M+BT+KT^2}, \quad (28a)$$

$$j_k^* := \frac{q_k^* - 3q_{k-1} + 3q_{k-2} - q_{k-3}}{T^3}, \quad (28b)$$

$$a_{k-1} := \frac{q_{k-1} - 2q_{k-2} + q_{k-3}}{T^2}, \quad (28c)$$

$$v_{k-1} := \frac{q_{k-1} - q_{k-2}}{T}, \quad (28d)$$

$$\bar{V}_{b,k} := \frac{-V - v_{k-1} - (T+P)a_{k-1}}{T^2+PT}, \quad (28e)$$

$$\bar{V}_{t,k} := \frac{V - v_{k-1} - (T+P)a_{k-1}}{T^2+PT}, \quad (28f)$$

$$\bar{A}_{b,k} := \frac{-A - a_{k-1}}{T}, \quad (28g)$$

$$\bar{A}_{t,k} := \frac{A - a_{k-1}}{T}, \quad (28h)$$

$$\bar{J}_{b,k} := \mathrm{proj}_{[-J,-J_y]}\left(\frac{-Ha_{k-1} - J_s}{1+HT}\right), \quad (28i)$$

$$\bar{J}_{t,k} := \mathrm{proj}_{[J_y,J]}\left(\frac{-Ha_{k-1} + J_s}{1+HT}\right), \quad (28j)$$

$$\mathcal{L}_k := \left[\max\left(\bar{V}_{b,k}, \bar{A}_{b,k}, \bar{J}_{b,k}\right), \min\left(\bar{V}_{t,k}, \bar{A}_{t,k}, \bar{J}_{t,k}\right)\right], \quad (28k)$$

$$j_k := \mathrm{proj}_{\mathcal{L}_k}\left(j_k^*\right), \quad (28l)$$

$$q_k := 3q_{k-1} - 3q_{k-2} + q_{k-3} + T^3 j_k. \quad (28m)$$

Note that the algorithm (28) is something that can be directly implemented to control devices through translations into appropriate programming languages. The computational load of the algorithm (28) is almost negligible since it does not involve iterative computations.

The values for the parameters P and H should be chosen so that the algorithm (28) always has a unique solution. Specifically,

$$\max\left(\bar{V}_{b,k}, \bar{A}_{b,k}, \bar{J}_{b,k}\right) \le \min\left(\bar{V}_{t,k}, \bar{A}_{t,k}, \bar{J}_{t,k}\right). \quad (29)$$

is necessary and sufficient for the existence of the solution, assuring the non-emptiness of the set $\mathcal{L}_k$ appearing in Eq. (28k). To verify the condition (29), one needs to check nine (= 3×3) inequalities. One can easily see that, if $[v_{k-1}, a_{k-1}, j_{k-1}]^{\mathrm{T}}$ is included in the set defined by Eq. (8) and illustrated in **Fig. 3**, the following inequalities are satisfied:

$$\bar{A}_{b,k} \le 0 \le \bar{A}_{t,k},\ \bar{J}_{b,k} \le 0 \le \bar{J}_{t,k},\ \bar{V}_{b,k} < \bar{V}_{t,k}. \quad (30)$$

Among the nine inequalities required by Eq. (29), five are implied by Eq. (30). The remaining four inequalities are:

$$\bar{V}_{b,k} \le \bar{A}_{t,k},\ \bar{V}_{b,k} \le \bar{J}_{t,k},\ \bar{A}_{b,k} \le \bar{V}_{t,k},\ \bar{J}_{b,k} \le \bar{V}_{t,k}. \quad (31)$$

Through tedious but straightforward derivations (with the help of symbolic computation software programs such as Mathematica), one can see that the following condition is sufficient to satisfy Eq. (31):

$$P \ge \frac{A}{J} - T \wedge H \ge \frac{1}{P}. \quad (32)$$

That is, the values for the parameters P and H need to be chosen to satisfy Eq. (32) in the implementation of the algorithm (28). More specifically, P needs to be set slightly larger than $A/J - T$ because setting a larger P could lead to undesirable deceleration before reaching the velocity limits $\pm V$. Regarding H, as mentioned in Section 3.2, it should be smaller to achieve higher responsiveness, but it must be large enough not only to suppress vibrations but also to satisfy Eq. (32).

3.4. Properties of the Controller

The behavior of the robot in contact with a stiff environment is the main concern in force control applications. The proposed controller (6), of which the discrete-time representation is Eq. (28), is intended to alleviate the concern in comparison to the conventional simple controller (5), but it should be noted that the stability is not guaranteed with the proposed controller. Recall that the proposed controller (6) combines a linear controller (5) with some limiters, making the controller nonlinear. It is obvious that incorporating limiters, in principle, cannot alter an unstable system into a stable system, especially in the sense of Lyapunov stability. The following discussion shows that the limiters in the controller result in stable limit cycles in the systems when they are divergent without the limiters.

The following discussion is based on the conventional describing function method. The describing function of the proposed controller (6), or its discrete-time representation (Eq. (28)), cannot be analytically obtained. However, it can be numerically obtained by providing sinusoidal inputs with different amplitudes and frequencies. Let us consider the sequence $\{f_k\}_{k\in\mathbb{Z}}$, where

$$f_k = U\cos(k\omega T), \quad (33)$$

which is a sinusoidal signal with the amplitude $U > 0$ and the frequency $\omega > 0$. Let us assume that, with the input sequence $\{f_k\}_{k\in\mathbb{Z}}$, the algorithm (28) provides an output sequence $\{q_k\}_{k\in\mathbb{Z}}$. Based on these sequences, the describing function $\Psi : \mathbb{R}_+ \times \mathbb{R}_+ \to \mathbb{C}$ of the algorithm (28) can be numerically obtained as follows:

$$\Psi(U,\omega) \triangleq \frac{\sum_{k=n}^{n+\frac{2\pi}{\omega}} q_k\left(\cos(k\omega T) - j\sin(k\omega T)\right)}{U\sum_{k=n}^{n+\frac{2\pi}{\omega}} \cos(k\omega T)^2}. \quad (34)$$

With the algorithm (28), if the input amplitude U is small enough, the jerk j_k does not reach the upper bounds in the algorithm, and thus the output $\{q_k\}_{k\in\mathbb{Z}}$ becomes equivalent to the output of the linear controller (5), which is the algorithm (28) with the limits $\{V, A, J, J_s, J_y\}$ set to be the infinity. Therefore, one can see that the func-

tion $\Psi(U, \omega)$ has the following property:

$$\lim_{U \to 0} \Psi(U, \omega) = \frac{1}{K - M\omega^2 + jB\omega}. \quad \ldots\ldots (35)$$

Here, note that the right-hand side of Eq. (35) is the transfer function of the linear controller (5) in the frequency domain. In addition, when the input amplitude U becomes larger, the signal amplitude would more frequently hit the upper bounds, and the ratio of the output amplitude against the input amplitude U would decrease. Therefore, $\Psi(U, \omega)$ also has the following property:

$$\frac{\partial |\Psi(U, \omega)|}{\partial U} < 0. \quad \ldots\ldots\ldots\ldots (36)$$

Recall that the output q of the algorithm (28) is sent to the robot controller as the position command. Let $P(s)$ be the transfer function from the position command q to the robot position p. Let K_e be the stiffness of the environment in contact with the robot's end-effector. Then, the force f, which is used as the input to the algorithm (28), satisfies $f = -K_e p$, and the open-loop transfer function of the system in the frequency domain is $-K_e P(j\omega)\Psi(U, \omega)$. By using this, we can see that the oscillation of the force f with the angular frequency ω and the amplitude U persists if the following harmonic balance equation [25] is satisfied:

$$K_e P(j\omega)\Psi(U, \omega) = -1 + 0j. \quad \ldots\ldots\ldots (37)$$

In addition, because of the property (36), if the magnitude of the oscillation is larger or smaller than U satisfying Eq. (37), it would decrease or increase, respectively, until it reaches U. It means that the limit cycle with the angular frequency ω and the amplitude U satisfying Eq. (37) is stable. The existence of the limit cycle can also be explained in a similar light as in Section 5.4.3 of [26].

The obtained conclusion is that the admittance controller without limiters may be unstable and divergent, while the one combined with the limiters results in stable limit cycles and does not diverge. Whether the limit cycle is practically acceptable or not would depend on its amplitude and frequency and also on the application. The parameters should be chosen so that at least the amplitude of the limit cycle is small enough, although tuning guidelines of parameters are still unclear. Experiments in the next section empirically show that the oscillation can be made acceptably small with a robot with 6 ms deadtime by careful tuning of parameters.

4. Experiment

4.1. Experimental Setup

The six-DOF collaborative robot UR3e (Universal Robots) shown in **Fig. 4** was used in the experiments. Its payload capacity is 3 kg, and its maximum reach is 500 mm from the center of Joint 0. Universal Robots provides an API named real-time data exchange (RTDE) to allow communication between the dedicated robot controller and user programs running on a PC through TCP/IP

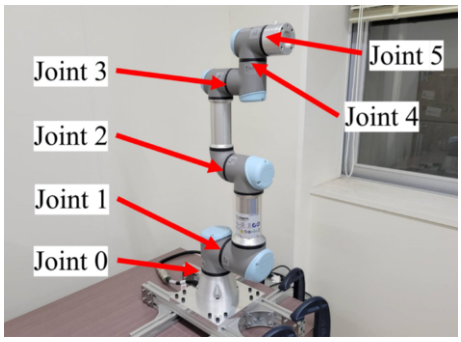

Fig. 4. Experimental setup (UR3e, Universal Robots) and its joint numbers.

at the cycle of $T = 0.002$ s. This study used the RTDE function `speedJ` to send the velocity command v ($= \dot{q}$) to the robot (the second argument A^*, the maximum acceleration, of `speedJ` was set as $A^* = 5$ rad/s^2). We did not use the position command q directly because the function `servoJ`, which is to send position commands, caused significant latency between the sent command q and the measured position p_s, which resulted in low stability of admittance control.

We estimated the external force f, which is necessary for admittance controllers, using the motor current and pre-calibrated weight distribution of the robot. Specifically, we computed the input force f in the following procedure:

$$\hat{f}_c := \hat{k}_c c, \quad \ldots\ldots\ldots\ldots\ldots (38a)$$

$$f := \mathrm{dzn}_{[-F,F]}\left(-\hat{f}_c + f_g(p_s)\right), \quad \ldots\ldots (38b)$$

where $\hat{f}_c$ is the estimated torque generated by the motor, $\hat{k}_c$ is the estimated torque constant of the motor, c is the motor torque obtained by the function `getActualCurrent`, p_s is the joint angle obtained by the function `getActualQ`, and $f_g(p)$ is the torque caused by the gravity. The use of the deadzone function in Eq. (38) is to attenuate the influence of the noise and the inertia. The parameters needed to calculate $f_g(p)$ were chosen through some preliminary experiments. The torque constants $\hat{k}_t$ were estimated as $\{\hat{k}_{t0}, \hat{k}_{t1}, \hat{k}_{t2}, \hat{k}_{t3}, \hat{k}_{t4}, \hat{k}_{t5}\} = \{18, 18, 9.5, 4, 4, 4\}$ Nm/A.

For the purpose of comparison, we used the following two controllers:

- cP: proposed controller (28)
- cN: controller cP with a simple jerk limiter, $\mathcal{J} = [-J, J]$

Unless otherwise specified, the parameters were set as shown in **Table 1**.

Figure 5 illustrates relations among some signals relevant to the dedicated robot controller of UR3e. The robot controller receives the velocity command v from the PC through TCP/IP through an RTDE function `speedJ`. The function receives another argument, which is an acceleration limit A^*. It then produces the motor current c, which

Table 1. Parameters used in the experiments.

Symbols	Physical meaning	Value and units
M	The virtual inertia	0.0625 kg · m^2 ($= B^2/4K$)
B	The virtual viscosity	0.5 Ns/rad
K	The virtual stiffness	1 N/rad
V	The velocity limit	1.5 rad/s
A	The acceleration limit	5 rad/s^2
J	The jerk limit	300 rad/s^3
P	The time constant for the velocity limit	0.015 s
H	The slope of the jerk limit shown in **Fig. 2(c)**	3000 s^{-1}
J_s	The intercept of the jerk limit shown in **Fig. 2(c)**	500 rad/s^3
J_y	The jerk limit at high acceleration	30 rad/s^3

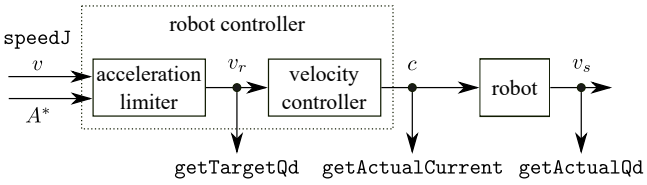

Fig. 5. Relation among the velocity command v, the modified "target velocity" v_r subject to the acceleration limit A^*, the motor current c, and the measured velocity v_s in the experimental setup. Relevant RTDE functions are also shown.

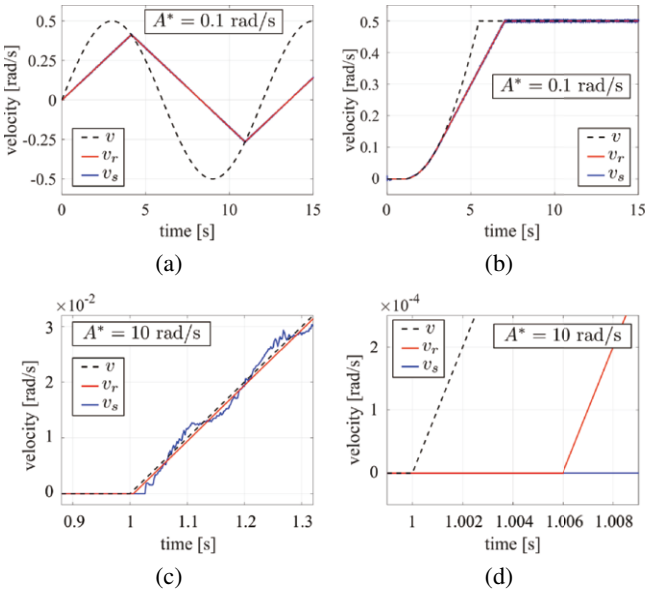

Fig. 6. Velocity command v sent to the robot controller, the "target velocity" v_r obtained from the robot controller, and the measured joint velocity v_s. (a) A sin wave was commanded by v with the acceleration limit of `speedJ` set as $A^* = 0.1$ rad/s^2. (b) A parabola $(t-1)^2/40$ with an upper bound 0.5 rad/s was commanded by v with $A^* = 0.1$ rad/s^2. (c) The command v was changed from 0 rad/s with $A^* = 10$ rad/s^2. (d) An enlarged version of (c).

can be monitored by the function `getActualCurrent`, and the resultant joint velocity is obtained by the function `getActualQd`. In addition, there is a function `getTargetQd` to monitor a "target velocity," which we hereafter refer to as v_r. It is presumably a modified velocity command used within the controller.

Figure 6 shows the results of some preliminary experiments to check how large a deadtime exists in the controller. **Fig. 6(a)** shows the results of a trial where v was a sinusoidal wave with $A^* = 0.1$ rad/s^2 and **Fig. 6(b)** shows the results of a trial where $v = \min(0.5, (t-1)^2/40)$ [rad/s] with $A^* = 0.1$ rad/s^2. It can be seen that the measured joint velocity v_s follows the modified velocity v_r, not the original velocity command v, and that v_r tracks v as $|\dot{v}|$ is smaller than A^*. **Figs. 6(c)** and **(d)** show the result of trials with $A^* = 10$ rad/s^2 plotted in different time scales. They show that there is a time delay of approximately 6 ms between v and v_r. It means that the deadtime of approximately 6 ms exists in the robot controller. Note that the proposed controller does not explicitly use the information on the deadtime of the robot, and these preliminary experiments were only for reference purposes.

4.2. Experiment I: Moved by Hand

In the first set of experiments, the experimenter moved the robot by pushing the end-effector by hand. The controllers cN and cP were implemented to Joint 0. The parameter F was set as $F = 28$ Nm. The desired position was set as $p_d = 0$ throughout the experiments.

In the beginning, the robot was stationary at $p_d = 0$ as shown in **Fig. 7(a)**. Then, the experimenter pushed the

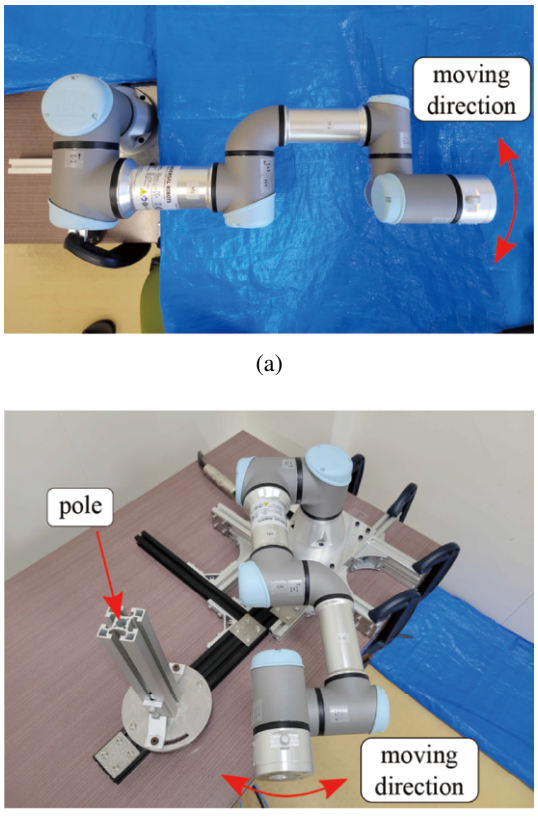

Fig. 7. Configurations for (a) Experiment I and (b) Experiment II.

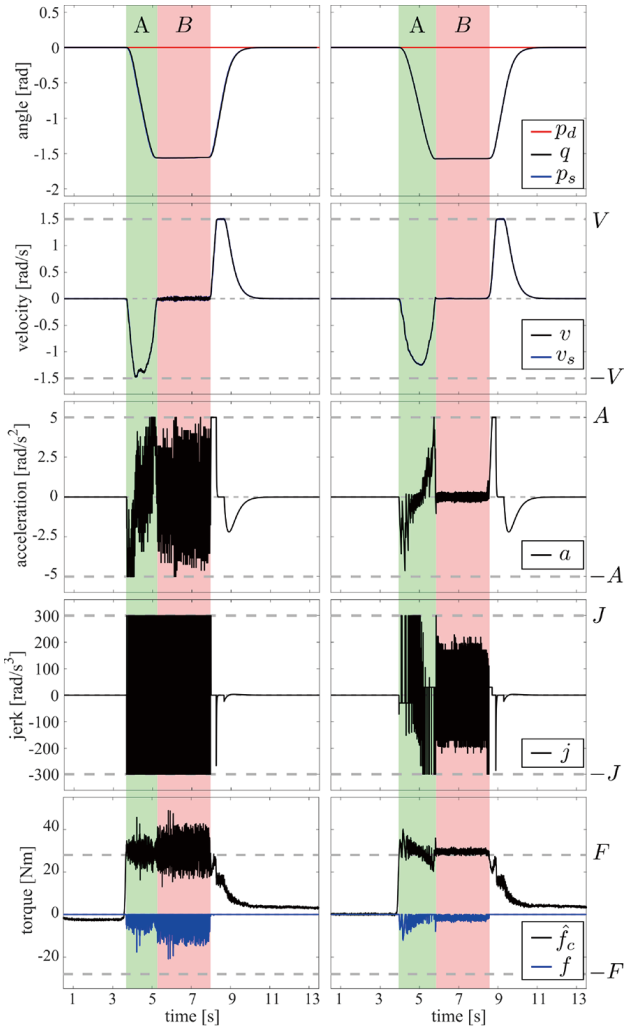

(a) Controller cN (b) Controller cP

Fig. 8. Results of Experiment I. In Period A, the experimenter moved the robot by hand. In Period B, he held the robot and stopped its movement. After Period B, he took his hand away from the robot.

robot by hand on the end-effector for a while (Period A). After that, the experimenter stopped and firmly grasped the end-effector (Period B). Finally, the experimenter put his hand away from the end-effector.

The results are shown in **Fig. 8**. In Period A, the robot was being moved by the external force, the generated torque $\hat{f}_c$, and the commanded acceleration a vibrated, but the amplitude was smaller with cP than with cN. This can be seen as the effect of cP bounding the commanded jerk j. The difference was more distinct in Period B, in which the vibrations are much smaller with cP than with cN, especially in the commanded acceleration a. In fact, the actuator generated a noisy sound with cN but not with cP, and the experimenter did not feel the vibration with cP while grasping the robot. After Period B, the experimenter released the robot, and the robot position p converged smoothly to p_d with both controllers, as intended by the setting of the values of M, B, and K, resulting in the critical damping. **Table 2** shows data indicating the amplitudes of the vibration, which are the standard deviations

Table 2. Standard deviations of some signals Period B of Experiment I.

Signals	Controller cN	Controller cP
q [rad]	2.53×10^{-3}	6.91×10^{-4}
v [rad/s]	2.17×10^{-2}	0.18×10^{-2}
a [rad/s^2]	2.32	0.19
j [rad/s^3]	2.99×10^{2}	1.00×10^{2}
$\hat{f}_c$ [Nm]	7.21	0.81

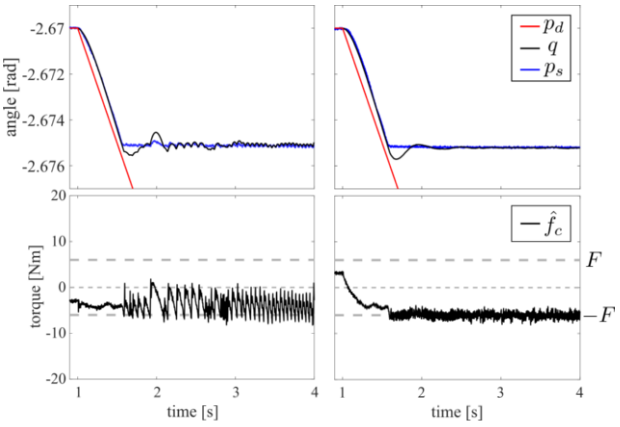

(a) Controller cN (b) Controller cP

Fig. 9. Results of Experiment II. The end-effector contacted the pole at around $t = 1.58$ s and it kept pushing after that.

of some signals in Period B. It shows that the vibration is smaller with the proposed controller cP than with cN.

Although it is not shown in the figures, when J was chosen larger, the vibration amplitude became larger, and the teaching pendant of UR3e displayed an error message.

4.3. Experiment II: Contact with Environment

The second set of experiments was conducted to investigate the performance of the proposed controller in contact with a rigid external object. As shown in **Fig. 7(b)**, an aluminum pole was fixed to the robot's base, and Joint 0 was controlled so that the end-effector gains contact with the pole. Specifically, p_d of Joint 0 was initially set as $p_d = -2.67$ rad, and from $t = 1$ s, p_d was varied with the velocity $\dot{p}_d = -0.01$ rad/s. The end-effector contacted the pole at around $t = 1.58$ s, and after that, the robot continued applying the force on the pole. The parameters were set as the same as in Experiment I, except that F was set as $F = 6$ Nm.

The results are shown in **Fig. 9**. The controller cN resulted in bouncing when the end-effector contacted the pole. In contrast, the controller cP maintained contact with the surface of the pole. Even with the controller cP, the force $\hat{f}_c$ vibrated with a small amplitude during the contact with the pole, as shown in **Fig. 9(b)**. No noisy sound, however, was heard from the actuator and the contact surface. **Table 3** shows some data indicating the amplitudes of the vibration, which are the standard deviations of some

Table 3. Standard deviations of some signals in the period from $t = 1.58$ s to 4.0 s of Experiment II.

Signals	Controller cN	Controller cP
q [rad]	1.65×10^{-4}	1.20×10^{-4}
v [rad/s]	4.88×10^{-3}	1.66×10^{-3}
a [rad/s^2]	0.60	0.19
j [rad/s^3]	1.55×10^{2}	0.96×10^{2}
$\hat{f}_c$ [Nm]	1.95	0.75

signals (not all are shown in **Fig. 9**) after the end-effector gained the contact with the pole. It is shown that the vibration is smaller with the proposed controller cP than with cN.

4.4. Experiment III: Moved by Hand with 6-DOF Control

In the third set of experiments, the controllers cN and cP were implemented in all joints of the robot with the setting $K = 0$. The experimenter grasped the end-effector and attempted to move the end-effector along a circular path in the task space. The controllers cN and cP were implemented independently to each joint. Because of the setting $K = 0$, the controller was supposed to behave as a mass-damper system illustrated in **Fig. 1(c)**. The parameter F was set as $\{F_0, F_1, F_2, F_3, F_4, F_5\} = \{4, 6, 3, 1, 0.5, 0.4\}$ Nm. The values of F were determined so that the experimenter was able to move the robot with a light hand, and also $|\hat{f}_e|$ does not exceed F during the motion as long as no external forces acted. Other parameters were set the same as in Experiment I for all joints.

The results are shown in **Fig. 10**. In **Fig. 10**, the three-dimensional graphs on the top show the trajectories of the end-effector in the task space, and the other graphs are $\hat{f}_c$ of the joints. With both controllers, the experimenter was able to make the robot move along a circle, and significant difference cannot be found between the trajectories resulted from cP and cN in **Fig. 10**. However, the magnitudes of vibration of $\hat{f}_c$ were smaller with the proposed controller cP than with the controller cN. In addition, with the controller cN, the experimenter heard a noisy sound from the actuators and felt a vibration in his hand, while with cP, he did not perceive sound or vibration. **Table 4** shows some data indicating the amplitudes of the vibration, which are the standard deviations of the actuator force $\hat{f}_c$ high-pass filtered at 15 Hz. It also shows that the vibration is smaller with cP than with cN.

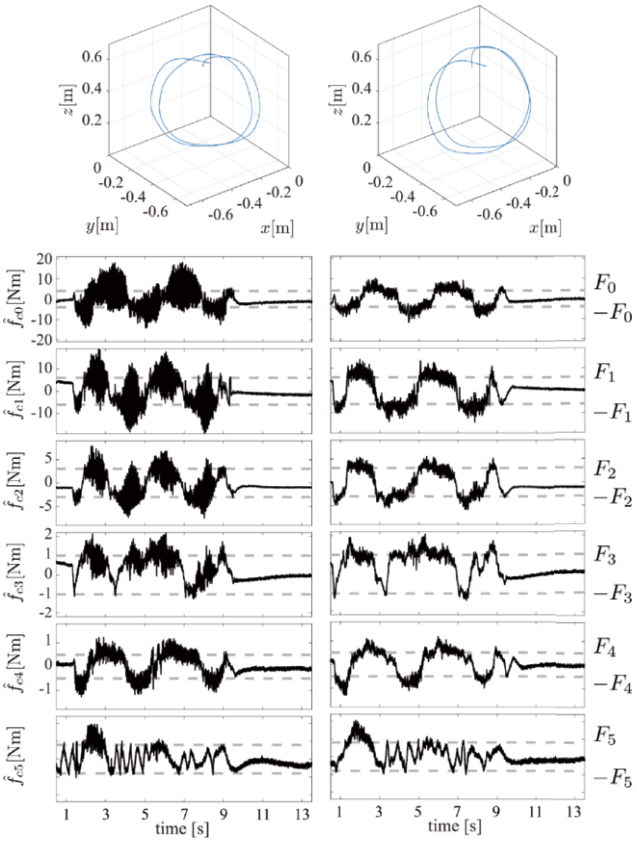

(a) Controller cN (b) Controller cP

Fig. 10. Results of Experiment III. The experimenter grasped the end-effector and moved it along a circle.

Table 4. Standard deviations of high-pass filtered $\hat{f}_c$ in the period from $t = 0$ s to 13 s of Experiment III.

Joint name	Controller cN	Controller cP
Joint 0	2.48 Nm	0.70 Nm
Joint 1	2.30 Nm	0.93 Nm
Joint 2	0.86 Nm	0.35 Nm
Joint 3	0.17 Nm	0.08 Nm
Joint 4	0.11 Nm	0.06 Nm
Joint 5	0.06 Nm	0.04 Nm

5. Conclusion

This paper has proposed an admittance control scheme for joint-level position-controlled robots. The controller has an elaborate discrete-time jerk limiter to limit the third derivative of the position command sent to the robot controller. It effectively suppresses the amplitude of oscillation presumably caused by the deadtime inside the robot controller, especially when the robot is in contact with external environments. The controller was validated with a UR3e robot, which has a 6 ms deadtime in the velocity-command mode.

Future work should address clarification of guidelines for tuning the parameters, especially those of the jerk limiter. In addition, extension of the controller to a task-space controller would also be necessary.

Acknowledgments

This work was supported by JSPS KAKENHI Grant Number JP21K04122.

References:

[1] D. A. Lawrence, "Impedance control stability properties in common implementations," Proc. of 1988 IEEE Int. Conf. on Robotics and Automation, Vol.2, pp. 1185-1190, 1988. https://doi.org/10.1109/ROBOT.1988.12222

[2] C. T. Landi et al., "Variable admittance control preventing undesired oscillating behaviors in physical human-robot interaction," 2017 IEEE/RSJ Int. Conf. on Intelligent Robots and Systems (IROS), pp. 3611-3616, 2017. https://doi.org/10.1109/IROS.2017.8206207

[3] Y. Sun et al., "Adaptive admittance control for safety-critical physical human robot collaboration," IFAC-PapersOnLine, Vol.56, No.2, pp. 1313-1318, 2023. https://doi.org/10.1016/j.ifacol.2023.10.1772

[4] T. Sun, Z. Wang, C. He, and L. Yang, "Adaptive robust admittance control of robots using duality principle-based impedance selection," Applied Sciences, Vol.12, No.23, Article No.12222, 2022. https://doi.org/10.3390/app122312222

[5] C. T. Landi, F. Ferraguti, L. Sabattini, C. Secchi, and C. Fantuzzi, "Admittance control parameter adaptation for physical human-robot interaction," 2017 IEEE Int. Conf. on Robotics and Automation (ICRA), pp. 2911-2916, 2017. https://doi.org/10.1109/ICRA.2017.7989338

[6] F. Dimeas and N. Aspragathos, "Online stability in human-robot cooperation with admittance control," IEEE Trans. on Haptics, Vol.9, No.2, pp. 267-278, 2016. https://doi.org/10.1109/TOH.2016.2518670

[7] B. Yao et al., "Sensorless and adaptive admittance control of industrial robot in physical human-robot interaction," Robotics and Computer-Integrated Manufacturing, Vol.51, pp. 158-168, 2018. https://doi.org/10.1016/j.rcim.2017.12.004

[8] G. Kang, H. S. Oh, J. K. Seo, U. Kim, and H. R. Choi, "Variable admittance control of robot manipulators based on human intention," IEEE/ASME Trans. on Mechatronics, Vol.24, No.3, pp. 1023-1032, 2019. https://doi.org/10.1109/TMECH.2019.2910237

[9] F. Ferraguti et al., "A variable admittance control strategy for stable physical human–robot interaction," The Int. J. of Robotics Research, Vol.38, No.6, pp. 747-765, 2019. https://doi.org/10.1177/0278364919840415

[10] Z. Chen, Q. Guo, T. Li, Y. Yan, and D. Jiang, "Gait prediction and variable admittance control for lower limb exoskeleton with measurement delay and extended-state-observer," IEEE Trans. on Neural Networks and Learning Systems, Vol.34, No.11, pp. 8693-8706, 2023. https://doi.org/10.1109/TNNLS.2022.3152255

[11] C. Liu, Y. He, X. Chen, and H. Cao, "Adaptive enhanced admittance force-tracking controller design for highly dynamic interactive tasks," Industrial Robot, Vol.49, No.5, pp. 903-912, 2022. https://doi.org/10.1108/IR-10-2021-0222

[12] K. Haninger, M. Radke, A. Vick, and J. Krüger, "Towards high-payload admittance control for manual guidance with environmental contact," IEEE Robotics and Automation Letters, Vol.7, No.2, pp. 4275-4282, 2022. https://doi.org/10.1109/LRA.2022.3150051

[13] R. Kikuuwe, "A sliding-mode-like position controller for admittance control with bounded actuator force," IEEE/ASME Trans. on Mechatronics, Vol.19, No.5, pp. 1489-1500, 2014. https://doi.org/10.1109/TMECH.2013.2286411

[14] R. Kikuuwe, "Torque-bounded admittance control realized by a set-valued algebraic feedback," IEEE Trans. on Robotics, Vol.35, No.5, pp. 1136-1149, 2019. https://doi.org/10.1109/TRO.2019.2920069

[15] M. T. S. Aung and R. Kikuuwe, "Stability enhancement of admittance control with acceleration feedback and friction compensation," Mechatronics, Vol.45, pp. 110-118, 2017. https://doi.org/10.1016/j.mechatronics.2017.06.011

[16] Y. Aydin, O. Tokatli, V. Patoglu, and C. Basdogan, "Stable physical human-robot interaction using fractional order admittance control," IEEE Trans. on Haptics, Vol.11, No.3, pp. 464-475, 2018. https://doi.org/10.1109/TOH.2018.2810871

[17] Y. Aydin, O. Tokatli, V. Patoglu, and C. Basdogan, "Fractional order admittance control for physical human-robot interaction," 2017 IEEE World Haptics Conf. (WHC), pp. 257-262, 2017. https://doi.org/10.1109/WHC.2017.7989911

[18] K. Li, Y. He, K. Li, and C. Liu, "Adaptive fractional-order admittance control for force tracking in highly dynamic unknown environments," Industrial Robot, Vol.50, No.3, pp. 530-541, 2023. https://doi.org/10.1108/IR-09-2022-0244

[19] A. Morbi and M. Ahmadi, "Safely rendering small impedances in admittance-controlled haptic devices," IEEE/ASME Trans. on Mechatronics, Vol.21, No.3, pp. 1272-1280, 2016. https://doi.org/10.1109/TMECH.2015.2506994

[20] A. Lecours and C. Gosselin, "Computed-torque control of a four-degree-of-freedom admittance controlled intelligent assist device," J. P. Desai, G. Dudek, O. Khatib, and V. Kumar (Eds.), "Experimental Robotics: The 13th International Symposium on Experimental Robotics," pp. 635-649, Springer, 2013. https://doi.org/10.1007/978-3-319-00065-7_43

[21] R. Kikuuwe and B. Brogliato, "A new representation of systems with frictional unilateral constraints and its Baumgarte-like relaxation," Multibody System Dynamics, Vol.39, No.3, pp. 267-290, 2017. https://doi.org/10.1007/s11044-015-9491-6

[22] B. Brogliato, A. Daniilidis, C. Lemaréchal, and V. Acary, "On the equivalence between complementarity systems, projected systems and differential inclusions," Systems & Control Letters, Vol.55, No.1, pp. 45-51, 2006. https://doi.org/10.1016/j.sysconle.2005.04.015

[23] V. Acary and B. Brogliato, "Numerical Methods for Nonsmooth Dynamical Systems: Applications in Mechanics and Electronics," Springer, 2008. https://doi.org/10.1007/978-3-540-75392-6

[24] H. H. Bauschke and P. L. Combettes, "Convex Analysis and Monotone Operator Theory in Hilbert Spaces," 2nd edition, Springer, 2017. https://doi.org/10.1007/978-3-319-48311-5

[25] H. K. Khalil, "Nonlinear Systems," 3rd edition, Prentice Hall, 2002.

[26] J.-J. E. Slotine and W. Li, "Applied Nonlinear Control," Prentice Hall, 1990.

Appendix A. Derivation from Eq. (16) to Eq. (19)

Equation (19) can be derived from Eq. (16) as follows:

$$
\begin{aligned}
(16) \iff\ & j_k \in j_k^* - \mathcal{N}_{\mathcal{V}}\big(T\,(Tj_k + a_{k-1}) + v_{k-1} \\
& + P\,(Tj_k + a_{k-1})\big) \\
& - \mathcal{N}_{\mathcal{A}}\,(Tj_k + a_{k-1}) \\
& - \mathcal{N}_{\mathcal{J}(Tj_k + a_{k-1})}\,(j_k)\,, \quad \ldots\ldots \quad (39a) \\
\iff\ & j_k \in j_k^* - \mathcal{N}_{\overline{\mathcal{V}}}\,(j_k) - \mathcal{N}_{\overline{\mathcal{A}}}\,(j_k) \\
& - \mathcal{N}_{\overline{\mathcal{J}}(a_{k-1})}\,(j_k)\,, \quad \ldots\ldots \quad (39b) \\
\iff\ & j_k \in j_k^* - \mathcal{N}_{\overline{\mathcal{V}} \cap \overline{\mathcal{A}} \cap \overline{\mathcal{J}}(a_{k-1})}\,(j_k)\,, \quad . \quad (39c) \\
\iff\ & j_k \in j_k^* - \mathcal{N}_{\mathcal{L}_k}\,(j_k)\,, \quad \ldots\ldots \quad (39d) \\
\iff\ & (19), \quad \ldots\ldots\ldots\ldots \quad (39e)
\end{aligned}
$$

where $\overline{\mathcal{V}}$, $\overline{\mathcal{A}}$, and $\overline{\mathcal{J}}(a_{k-1})$ are closed intervals defined as

$$
\overline{\mathcal{V}} \triangleq \left[\frac{-V - v_{k-1} - (T+P)a_{k-1}}{T^2 + PT}, \frac{V - v_{k-1} - (T+P)a_{k-1}}{T^2 + PT} \right] \quad (40)
$$

$$
\overline{\mathcal{A}} \triangleq \left[\frac{-A - a_{k-1}}{T}, \frac{A - a_{k-1}}{T} \right] \quad \ldots\ldots \quad (41)
$$

$$
\overline{\mathcal{J}}(a_{k-1}) \triangleq \left[\mathrm{proj}_{[-J,-J_y]}\left(\frac{-Ha_{k-1} - J_s}{1 + HT} \right), \mathrm{proj}_{[J_y,J]}\left(\frac{-Ha_{k-1} + J_s}{1 + HT} \right) \right]. \quad (42)
$$

Here, the derivation from Eqs. (39a) to (39b) can be explained by the following equivalences:

$$
\begin{aligned}
& j_k \in \mathcal{J}\left(T j_k + a_{k-1}\right) \\
& \iff \operatorname{proj}_{[-J,-J_y]}\left(-J_s - H a_{k-1} - H T J_k\right) \\
& \qquad \le j_k \le \operatorname{proj}_{[J_y,J]}\left(J_s - H a_{k-1} - H T J_k\right) \\
& \iff \Big((-J \le j_k) \wedge \big((-J_y \le j_k) \\
& \qquad \vee (-J_s - H a_{k-1} - H T j_k \le j_k)\big)\Big) \\
& \qquad \wedge \Big((J \ge j_k) \wedge \big((J_y \ge j_k) \\
& \qquad \vee (J_s - H a_{k-1} - H T j_k \ge j_k)\big)\Big) \\
& \iff \left((-J \le j_k) \wedge \left((-J_y \le j_k) \vee \left(\frac{-J_s - H a_{k-1}}{1 + HT} \le j_k\right)\right)\right) \\
& \qquad \wedge \left((J \ge j_k) \wedge \left((J_y \ge j_k) \vee \left(\frac{J_s - H a_{k-1}}{1 + HT} \ge j_k\right)\right)\right) \\
& \iff \operatorname{proj}_{[-J,-J_y]}\left(\frac{-J_s - H a_{k-1}}{1 + HT}\right) \\
& \qquad \le j_k \le \operatorname{proj}_{(J_y,J)}\left(\frac{J_s - H a_{k-1}}{1 + HT}\right) \\
& \iff j_k \in \overline{\mathcal{J}}\left(a_{k-1}\right). \qquad (43)
\end{aligned}
$$

The equivalence between Eqs. (39c) and (39d) can be easily seen by $\mathcal{L}_k = \overline{\mathcal{V}} \cap \overline{\mathcal{A}} \cap \overline{\mathcal{J}}(a_{k-1})$ by the definitions in Eqs. (26), (40), (41), and (42).

Name:
Ryusei Mae

ORCID:
0009-0004-2621-5015

Affiliation:
Master's Course Student, Graduate School of Advanced Science and Engineering, Hiroshima University

Address:
1-4-1 Kagamiyama, Higashi-hiroshima, Hiroshima 739-8527, Japan

Brief Biographical History:
2022 Received B.E. degree in Mechanical Engineering from Hiroshima University
2022- Master's Course Student, Graduate School of Advanced Science and Engineering, Hiroshima University

Name:
Ryo Kikuuwe

ORCID:
0000-0002-1500-6777

Affiliation:
Professor, Graduate School of Advanced Science and Engineering, Hiroshima University

Address:
1-4-1 Kagamiyama, Higashi-hiroshima, Hiroshima 739-8527, Japan

Brief Biographical History:
1998 Received B.S. degree in Mechanical Engineering from Kyoto University
2000 Received M.S. degree in Mechanical Engineering from Kyoto University
2003 Received Ph.D. (Eng.) degree in Mechanical Engineering from Kyoto University
2003-2007 Endowed-Chair Research Associate, Nagoya Institute of Technology
2007-2017 Associate Professor, Department of Mechanical Engineering, Kyushu University
2014-2015 Visiting Researcher, Inria Grenoble Rhône-Alpes
2017- Professor, Hiroshima University

Main Works:
- R. Kikuuwe, Y. Yamamoto, and B. Brogliato, "Implicit Implementation of Nonsmooth Controllers to Nonsmooth Actuators," IEEE Trans. on Automatic Control, Vol.67, No.9, pp. 4645-4657, 2022.
- R. Kikuuwe, "Torque-Bounded Admittance Control Realized by a Set-Valued Algebraic Feedback," IEEE Trans. on Robotics, Vol.35, No.5, pp. 1136-1149, 2019.

Membership in Academic Societies:
- The Robotics Society of Japan (RSJ)
- The Japan Society of Mechanical Engineers (JSME)
- The Society of Instrument and Control Engineers (SICE)
- The Virtual Reality Society of Japan (VRSJ)